

MR Imaging of Diffusion of ^3He Gas in Healthy and Diseased Lungs

Brian T. Saam,¹ Dmitriy A. Yablonskiy,^{1,2} Vikram D. Kodibagkar,¹ Jason C. Leawoods,¹ David S. Gierada,³ Joel D. Cooper,⁴ Stephen S. Lefrak,⁵ and Mark S. Conradi^{1,2*}

Hyperpolarized ^3He gas MRI was used to form maps of the effective diffusivity of gas in human lungs. Images of diffusion as well as spin density are presented from a study of 11 healthy volunteers and 5 patients with severe emphysema. The effective rate of diffusion, D_e , of the gas is reduced by the alveolar walls; tissue destruction in emphysema is hypothesized to result in larger D_e . Indeed, the mean value of D_e in the emphysematous lungs is found here to be about 2.5 times that of healthy lungs, although still smaller than the unrestricted diffusivity of ^3He in free air. Histograms of D_e values across coronal slices are presented. The results are discussed in terms of spatial variations, variations among individuals, healthy and diseased, and variations due to changes in lung volume. Magn Reson Med 44:174–179, 2000. © 2000 Wiley-Liss, Inc.

Key words: hyperpolarized gas; gas; ^3He ; diffusion; lungs

The rapid development of hyperpolarized (HP) gas MR imaging has resulted from combined advances in the physics of optical pumping, affordable diode laser arrays, and MRI strategies for optimum use of the nonrenewable spin magnetization. High spatial resolution HP-gas imaging has yielded remarkable images, showing many levels of airway branching (1). In humans, the appearance of healthy and diseased lungs has been compared (2,3). Our own work has focused on high temporal resolution to image the ventilatory function of the lungs (4). All of these studies have used spin density (spin magnetization) as the imaged quantity.

The diffusion coefficient D_e (also known as rate of diffusion and diffusivity) and local dephasing time T_2^* of HP ^3He and ^{129}Xe have been measured recently (5–7) for use as image contrast parameters. The studies of D_e and T_2^* were also intended to determine how these quantities might confound spin density imaging and to establish optimum imaging parameters. Clearly, T_2^* sets an upper limit to MR signal time duration using gradient recalled echoes, and D_e results in a minimum voxel linear dimension for a given time (4). We note that diffusion in the present context refers to Brownian motion of the gas. He-

lium is virtually insoluble (8), so dissolution into tissue, lung fluid, or blood is not involved.

There is also important information in the spatially resolved maps of D_e and T_2^* . Here we report the results of spatially resolved measurements of D_e in healthy and diseased human lungs; the T_2^* variations are not discussed. We show that the effective diffusivity D_e is substantially increased in emphysematous lungs.

RESTRICTED DIFFUSION

At 1 atmosphere pressure and room temperature, the rate of self-diffusion of pure ^3He is $1.9 \text{ cm}^2/\text{s}$ (9), while the rate for very dilute ^3He in air (or N_2) is about $0.83 \text{ cm}^2/\text{s}$ (10,11). Dilute ^3He in N_2 is a good approximation to the gas in lung MRI, in that typically 0.5 L STP of ^3He is delivered to a patient with 6 L total lung volume. The rms atomic displacement (Brownian motion) along a single axis during time t is given by $\Delta X_{\text{rms}} = (2Dt)^{1/2}$. During a typical 5-ms duration imaging sequence, the rms displacement of ^3He through N_2 will be 0.9 mm. The above estimate is only appropriate in free (unbounded) gas, or where the boundaries are much further separated than 0.9 mm. The alveoli in healthy lungs may be approximated as spheres of approximately 0.15 mm radius, indicating that the diffusion of ^3He in lung tissue will be substantially impeded by collisions with alveolar walls. Indeed, our measurements in humans indicate a diffusivity of about $0.85 \text{ cm}^2/\text{s}$ in the trachea, compared to about $0.2 \text{ cm}^2/\text{s}$ in healthy lung tissue; similar values occur in guinea pig lungs (5).

We consider the lung a porous structure, a network of interconnected, approximately spherical compartments (alveoli). At very short times t , for which most gas atoms will not encounter the compartment walls, one expects the measured diffusivity to be that of free gas. For ^3He in N_2 inside human lungs, this corresponds to time $t \leq 0.13 \text{ ms}$. For longer times, such as the 5 ms typical of gas MRI pulse sequences, the atoms will move through the porous structure with a reduced, effective diffusivity, D_e (also known as apparent diffusion coefficient, ADC). For a statistically homogeneous porous structure, the value of D_e will be independent of the time duration t , provided that t exceeds the characteristic value $\ell^2/2D_e$, where ℓ is the longest characteristic length of the porous structure (12). In the present context, we associate ℓ with the mean alveolar diameter. We note that the present measurements use a diffusion-sensitizing gradient of 7.5 ms duration and are thus in the long time limit.

In the long time limit relevant to gas MRI, the value of D_e will depend on the sizes of the compartments (alveoli) as well as the sizes and the connectivity of the pores between the compartments (13,14). While the increase in mean

¹Department of Physics, CB 1105, Washington University, St. Louis, Missouri.

²Department of Radiology, CB 8225, Washington University, St. Louis, Missouri.

³Department of Radiology, CB 8131, Washington University, St. Louis, Missouri.

⁴Department of Surgery, CB 8234, Washington University, St. Louis, Missouri.

⁵Department of Internal Medicine, CB 8306, Washington University, St. Louis, Missouri.

Grant sponsor: Whitaker Foundation.

*Correspondence to: Mark S. Conradi, Washington University, Campus Box 1105, One Brookings Drive, St. Louis, MO 63130.
E-mail: msc@howdy.wustl.edu

Received 15 October 1999; revised 20 April 2000; accepted 21 April 2000.

© 2000 Wiley-Liss, Inc.

compartment size in emphysema is well known, little is known about changes in the network of connecting pores and pathways (e.g., alveolar ducts and pores of Kohn), but both are equally important to the effective diffusivity of the gas.

We emphasize that the effective diffusivity (in the limit of long times, as applies here) depends on the connecting pores and pathways, and not just the size of the compartments. For example, if the compartments were closed (not interconnected), the effective diffusivity ($\overline{X^2}/2t$) would be zero at large time, because the mean square displacement would be limited by the square of the compartment size.

A scaling argument also shows that the effective diffusivity depends on more than just the compartment size. Consider two pieces of lung tissue which are self-similar, but with B having twice the linear dimension scale of A in all three directions. Thus, the mean alveolar diameter, pore diameter, etc., of B is double that of A . Correspondingly, the mean alveolar volume of B is eight times that of A . Dimensionless quantities are equal in A and B , such as the fraction of total volume available to the gas. In the long time limit (for both A and B), the effective diffusivities in A and B will be equal. This is an immediate result of the absence of a relevant length scale in the long time limit. A second view involves the tortuosity, as discussed in Ref. 12. There it is shown that the effective diffusivity at long times is equal to the diffusion coefficient of the free gas divided by the tortuosity factor, a dimensionless quantity expressing the effect of the compartments and pores. Since tortuosity is dimensionless, it is the same in tissues A and B , and so is the effective diffusivity. Thus, the effective diffusivity depends on more than simply the sizes of the compartments.

The defining characteristic of emphysema is widespread destruction of alveolar wall tissue. Thus, we hypothesize that the effective diffusivity D_e of ^3He gas in emphysematous regions of lung will be increased compared to D_e in healthy lung tissue. The results presented here show that this is indeed the case.

EXPERIMENTS

Helium-3 gas was laser polarized using the technique of rubidium optical depopulation pumping and spin exchange between ^3He nuclear spins and the polarized Rb electron spins (15), with equipment constructed in the research group. Pyrex glass cells at 10 atm pressure yielded 0.45 L STP of ^3He at typically 40% spin polarization. The cells were transported 4 km to the imager in a 40 G field created by battery-powered Helmholtz coils.

The subjects were imaged using a 1.5 T whole-body MR scanner (Siemens Vision Magnetom, South Iselin, NJ) with a Helmholtz rf coil pair (one under the supine subject's back and one above the chest). The coils served for imaging both proton nuclei and ^3He , with retuning accomplished without disturbing the subject. Using proton NMR (63.63 MHz), the magnetic field was shimmed and a full set of coronal slices obtained at breathhold. Two of the slices were selected for subsequent diffusion imaging, with the anterior slice typically capturing the trachea and the other slice 3 cm posterior.

The imager and RF coils were then switched to ^3He . The polarized gas was released from the glass cell into a flexible polyethylene bag that had been previously purged of all O_2 and preloaded with 1.5–2 L of nitrogen. The subject inhaled the gas from the bag as a single bolus and ^3He MRI data acquisition at 48.47 MHz was started about 1 s later.

The pulse sequence used three 2D gradient echo sequences combined together so that each of the three has the same small-angle RF pulse, the same slice selection, phase encode, and read-out gradients. Data were collected in the interleaved manner by collecting the same line in k -space for all three images prior to stepping to the next line. This ensures reduced sensitivity to possible motion artifacts. Also, central reordering was used to reduce the possible influence of signal decay during acquisition. The gradient echo formation times TE (measured from each RF pulse) were 4.2, 11.7, and 11.7 ms; the third image also incorporated a diffusion-sensitizing gradient waveform, applied along the phase-encode direction (subject's left to right). The diffusivity in the lung has been found to be isotropic (7). The posterior slice and then the anterior slice were imaged in 6 s during the initial breathhold; after a 4-s delay to allow partial exhale, breathhold was resumed and the same two slices were imaged again. Most of the healthy volunteers were able to perform the above breathing maneuvers. Some patients could not inhale the full contents of the gas-filled bag; none of the patients could perform the second breathhold. Thus, only images at nearly full inspiration are reported here for patients.

The ^3He images used a slice thickness of 10 mm and the in-plane resolution was 7 mm \times 7 mm (450 mm field of view with 64 \times 64 k -space samples). For smaller subjects, this was reduced to 6.25 mm \times 6.25 mm in-plane resolution (400 mm field of view). Each of the 64 lines in k -space used an RF excitation of about 7°, allowing for repeated acquisition from the same spins.

The diffusion-sensitizing gradient waveform lasted 7.5 ms; the diffusion reported here is proportional to the mean-squared displacement during approximately that time. The trapezoidal pulse was crafted to have zero first moment, so as to be insensitive to constant velocity gas motions, as might occur from incomplete breathhold. The gradient waveform is essentially a pair of bipolar pulses back-to-back with mirror symmetry about the center of the composite pulse. Thus, the diffusivity measurements are insensitive to patient and cardiac motions and to convection of the gas. Further, it is important to note that the diffusivity of the gas is large (0.1–0.85 cm²/s), so that the displacement due to diffusion is always much larger than the displacements arising from the above sources. Compared to measurements of the relatively small diffusivity of water in tissue, the present measurements are comparatively straightforward.

The effective diffusivity D_e was determined on a pixel-by-pixel basis using

$$M_3/M_2 = \exp(-bD_e), \quad [1]$$

where M_3 and M_2 are the pixel intensities from the third and second interleaved images (identical except for diffusion-sensitizing gradient), respectively. Only those pixels

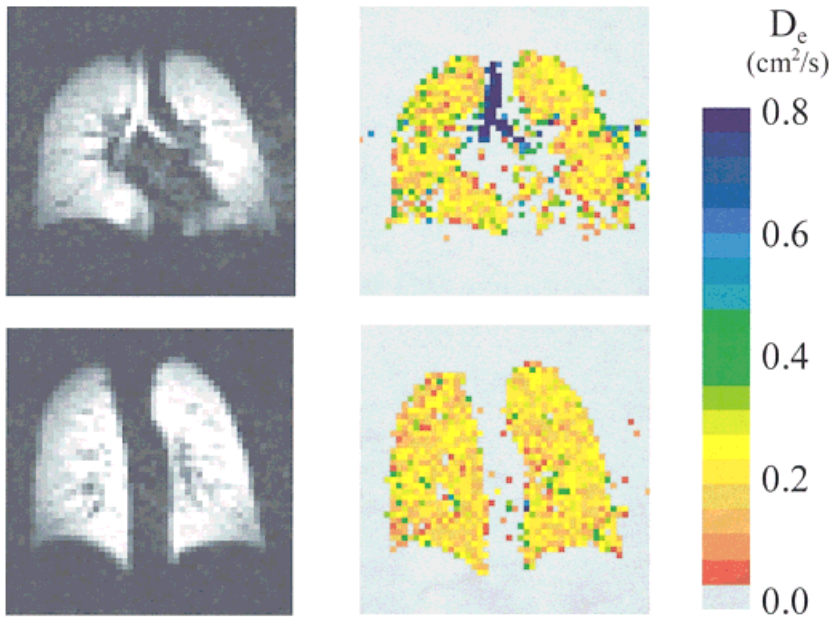


FIG. 1. Spin density (left) and diffusion (right) hyperpolarized ^3He coronal images from a healthy, 32-year-old male volunteer. The upper panels are from an anterior slice including the trachea (appears purple at right); the lower panels are from a posterior slice. All images are at nearly full inspiration. The very uniform diffusivity evident here is typical of the healthy volunteers.

for which the intensity in the second image exceeded the maximum noise were so analyzed; all other pixels were assigned the value of zero and appear as gray in the diffusion images. For the gradient waveform employed, the value of b was calculated using the approach of Karlicek and Lowe (16). For most of the healthy volunteers, the waveform amplitude was chosen so that $b = 2.75 \text{ s/cm}^2$. For most of the patients, the larger diffusion rates dictated that a smaller value of $b = 1.375 \text{ s/cm}^2$ be used. The noise in both the second and third images results in noise in the diffusivity maps. The rms noise from this source varies from subject to subject, but is approximately 6%. The first image ($\text{TE} = 4.2 \text{ ms}$) was used as a spin density map to reveal nonuniformities in ventilation. The SNR of the spin density image was generally 50:1. We note that the spin

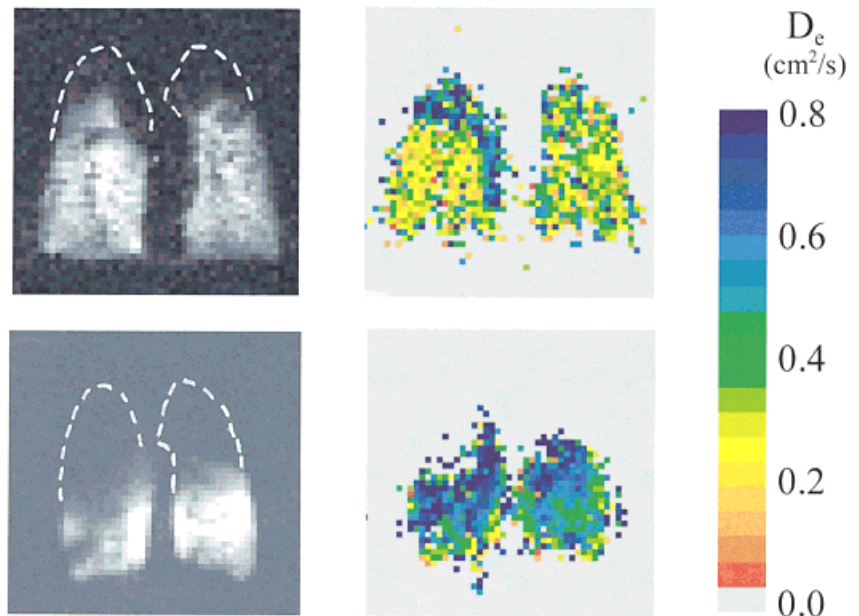
density images also reflect the RF field inhomogeneity of the Helmholtz RF coils.

Histograms of the effective diffusion values D_e across each coronal slice were prepared using the Microcal origin program on an Intel Pentium-based computer. Statistical analysis included calculation of the mean diffusivity $\overline{D_e}$, the rms width of the diffusivity distribution ΔD_e , and the fractional width $\Delta D_e / \overline{D_e}$. The rms width is defined by

$$\Delta D_e \equiv \left[\overline{(D_e - \overline{D_e})^2} \right]^{1/2}. \quad [2]$$

We note that all averages here give equal weighting to equal volume elements (except the discarded, poorly ventilated ones).

FIG. 2. Spin density (left) and diffusion (right) hyperpolarized ^3He coronal images from two patients with severe emphysema. All images are posterior slices (far from the trachea) at nearly full inspiration. The lower panels are from a 56-year-old woman with $\text{FEV}_1 = 13\%$ of predicted. The upper panels are from a 53-year-old male with $\text{FEV}_1 = 34\%$ of predicted. The color bar represents the scale for D_e values. The regions of high diffusivity result from tissue destruction characteristic of emphysema. The dashed outlines in the spin density images are taken from proton images of the same slices, revealing regions which do not receive substantial amounts of ^3He gas.



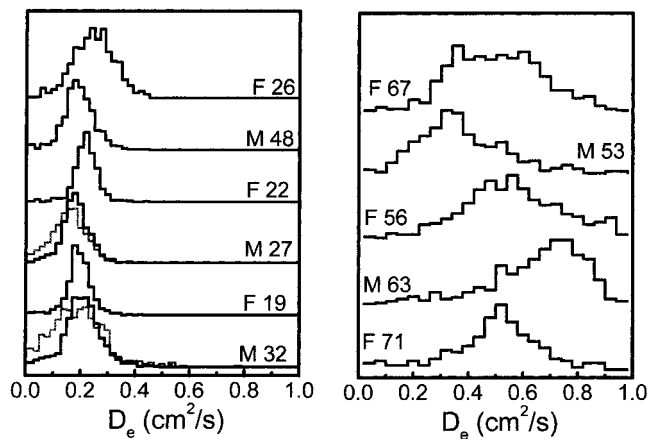


FIG. 3. Histograms of diffusivity D_e taken from the posterior coronal slice. The subject's sex and age are given. At left, the D_e of six healthy volunteers at nearly full inspiration (black) and at partial exhalation (gray, for two volunteers). At right, D_e histograms of five patients with severe emphysema. Note the substantially larger values of D_e for the patients than for the healthy volunteers. The complete results for healthy and diseased subjects are presented in Table 1.

Of the 11 healthy volunteers, nine were from 19 to 32 years old, four female. Two older male volunteers also participated, a 55-year-old who had smoked $\frac{1}{2}$ pack of cigarettes per day in college and a 48-year-old nonsmoker. The five patients all suffered from severe emphysema and were part of the WU lung volume reduction surgery (LVRS) program. They were imaged typically 5 days prior to scheduled surgery. The patients were age 53–71 years and had FEV₁ (forced expiratory volume in the first second) values from 13–34% of predicted. All required additional O₂ upon exercise and three of five did so even at rest. None of the patients had α_1 -antitrypsin deficiency (17). X-ray CT images and perfusion scintigraphy indicated for all five that the disease was most severe in the upper lobes, typical of smoking-related emphysema. For LVRS, a relatively heterogeneous distribution of emphysema is preferred (18).

All procedures were performed with careful regard for subject safety. The procedures were approved by the WU IRB; informed consent was obtained from all subjects prior to all experiments.

RESULTS AND DISCUSSION

Diffusion maps and spin density images are presented in Figs. 1 and 2 for a healthy volunteer and two emphysema patients, respectively. Figure 1 displays both coronal slices of a healthy 32-year-old male volunteer. While there are differences among images of the healthy individuals, the data in Fig. 1 are typical. The diffusivity in the trachea (appears purple in the anterior slice) is 0.85 cm²/s; the color scale of Fig. 1 is slightly saturated at this high value of diffusivity. This is close to the value for dilute ^3He in free air or N₂, verifying the present methodology of diffusivity measurement. We note that the trachea is obvious in the diffusivity map, while it is not prominent in the spin density image, being obscured by nearby gas.

The histograms in Fig. 3 provide an easily accessible summary of the data, albeit with all spatial information suppressed. The data from six volunteers appear in Fig. 3 left, including the 32-year-old male of Fig. 1. The following features are evident from Table 1 and the diffusivity histograms. 1) For all of the voxels, D_e is less than that of free gas. This is also evident from the diffusion maps and demonstrates the reduction of diffusivity by the partial confinement of the gas by the alveoli. 2) The mean diffusivity values \bar{D}_e run from 0.17 to 0.25 cm²/s, approximately a factor of 4 smaller than D_e in free gas. 3) The distributions of diffusivity are narrow (for example, note the flat yellow appearance of the lower right panel of Fig. 1). A dimensionless measure of the peak width is the fractional width, $\Delta D_e / \bar{D}_e$ (rms width divided by mean value). For the healthy volunteers, the fractional width runs from 0.20 to 0.37. The narrowest distributions appeared in two females with small frames, ages 24 and 30; this may reflect that these subjects reached the highest level of inspiration from the fixed quantity of delivered gas and thus achieved greater uniformity of inflation. Neither of the older male volunteers was exceptional, as is evident from the summary of the diffusivity results in Table 1.

The color display of the diffusivity maps allows small changes in D_e to be detected. For four of our 11 healthy volunteers (but not that of Fig. 1) a trend is evident, with D_e increasing slightly towards the apices. Because the subject is supine, this is not a gravitational effect. This also implies that the distributions of D_e values in smaller regions of the lung may be even narrower than the overall distributions presented in the histograms here. No consistent anterior–posterior difference was observed, possibly because of the small 3 cm distance between the two slices.

The left side of Fig. 3 allows comparison of the distribution of D_e at nearly full inspiration (black curves) and after partial exhalation to approximately FRC (functional residual capacity, gray curves) for two of the healthy male volunteers. In both cases, the mean value of D_e decreases about 10%. Furthermore, the fractional width is substantially larger, increasing about 40% (see Fig. 3).

Table 1
Diffusivity Results From Posterior Coronal Slice

Sex, age	Healthy (H)/emphysema (E)	FEV ₁ (%)	D_e (cm ² /s)	ΔD_e (cm ² /s)	$\Delta D_e / \bar{D}_e$
M 23	H		0.185	0.060	0.32
F 30	H		0.247	0.050	0.20
F 19	H		0.185	0.048	0.26
F 26	H		0.235	0.075	0.32
M 24	H		0.205	0.063	0.31
M 23	H		0.179	0.061	0.34
F 24	H		0.208	0.046	0.22
M 55	H		0.238	0.066	0.28
M 48	H		0.182	0.059	0.32
M 32	H		0.202	0.074	0.37
M 27	H		0.172	0.051	0.30
F 71	E	28	0.477	0.166	0.35
F 67	E	19	0.483	0.159	0.33
F 56	E	13	0.521	0.175	0.36
M 53	E	29	0.387	0.212	0.55
M 63	E	34	0.630	0.180	0.29

In the absence of a model for the porous structure of the lungs, we make a very coarse estimate of the magnitude of change expected in \overline{D}_e upon exhalation, based on the change in mean alveolar size. We assume that \overline{D}_e is simply proportional to R^2 , where R is the average radius of the alveoli; this view neglects important aspects of the problem, such as connectivity (see discussion in Restricted Diffusion, above). The number of alveoli is constant, so the simplest assumption of equal radii for all alveoli leads to $R^3 \propto V$, the lung volume. Thus, for a lung initially inflated to 6.0 L with subsequent exhalation to 4.0 L, the radius changes by a factor of 0.87, giving a factor of 0.76 for the reduction in R^2 . The observed changes were never this large. Still, the calculation demonstrates that the expected change in average alveolar size is not large. A realistic calculation would need to incorporate the changes in the alveolar size and changes in the connectivity (specifically, tortuosity factor).

The posterior slices of diffusion maps and spin density images are presented in Fig. 2 for two patients with emphysema. The lower panels are from a 56-year-old female with $FEV_1 = 13\%$ of predicted (prior to administration of inhaled bronchodilator medication); the upper panels present a 53-year-old male with $FEV_1 = 34\%$ of predicted (prior) and with qualitatively less dyspnea. The spin density images demonstrate that the inspired ^3He was distributed very nonuniformly through the lungs. This is emphasized by the dashed outlines of the lungs, taken from proton scout scans of the same slices. In particular, there is essentially no gas reaching the apical regions; this is especially prominent in the lower panel and is typical of LVRS patients. The diffusivity D_e can only be determined in regions with sufficient ^3He signal.

The histograms of Fig. 3 right summarize the data from the five patients. The larger diffusivities encountered here dictate the use of histogram bins twice as large as for the healthy volunteers. The following features are apparent from the histograms: 1) Essentially all of the pixels have a smaller D_e than the free gas value of $0.83 \text{ cm}^2/\text{s}$. 2) The average diffusivity \overline{D}_e runs from 0.48 to $0.63 \text{ cm}^2/\text{s}$ (except for the 53-year-old male of the upper panels in Fig. 2), values approximately 2.5 times as large as in the healthy volunteers. This is the most important finding of the present work and confirms our hypothesis. 3) The widths ΔD_e of the distributions in the patients are substantially larger than for the healthy volunteers. On the other hand, the fractional widths $\Delta D_e/\overline{D}_e$ of the distributions of the patients are approximately 0.34 (again, excepting the 53-year-old male patient), not much larger than in the healthy lungs. Thus, the increased widths evident in Fig. 3 right (compare to healthy volunteers at left) primarily reflect the larger mean values; histograms of $\log D_e$ would have nearly the same widths for patients and healthy volunteers.

The diffusivity maps and corresponding spin density images have been examined for correlations. However, any correlations are subtle, at best. For example, in the upper right panel of Fig. 2 a region of high diffusivity appears as a vertical blue and purple stripe in the right lung. Comparison of the spin density and diffusivity maps reveals a region near the mediastinum which receives gas, despite

the high diffusivity (and apparent destruction of the tissue there).

As one ascends the lungs toward the apices, a trend is evident in the lower panels of Fig. 2: the diffusivity D_e increases while the spin density decreases. Eventually the spin density becomes too small for calculation of D_e ; these regions appear gray in the D_e map. This trend upon ascent toward the apices appears to varying extent in three of the five patients.

Diffusivity measurements have been reported recently, comparing control rats to rats with elastase-induced lung disease, a rat model of emphysema (19). Relatively small differences in the diffusivity are found between the two groups, with an approximately 20% increase in \overline{D}_e for the diseased lungs. Interestingly, the changes in rat D_e are only apparent at end expiratory volume and are insignificant at full inspiration. The changes reported here are much larger, possibly due to disease severity, and suggest that diffusion measurements of ^3He in lungs may have diagnostic value.

It would be very helpful to compare ^3He diffusivity maps to ^3He MRI images of ventilatory function (4) and X-ray CT images. Because CT images are most directly obtained as axial (transverse) slices and because the rapid EPI sequence suffers the least artifacts when performed on axial slices, we plan to acquire axial diffusivity maps in the future. In addition, as most of the patients show no ^3He in the apices, a restricted set of axial slices will more efficiently sample the ventilated regions of the lung. We also note that use of an ultrafast FLASH sequence could allow mapping of the entire lung in about 6 s, as opposed to the 2 slices obtained here (20).

CONCLUSIONS

In all cases the effective diffusivity D_e of HP ^3He gas in lung tissue is reduced by the alveolar walls below the value for dilute ^3He in free air or N_2 . In healthy volunteers, including the 48- and 55-year-old males, the distribution of D_e is narrow, with fractional width $\Delta D_e/\overline{D}_e \cong 0.3$. Small but real differences between the healthy volunteers appear, including variation of the mean diffusivity \overline{D}_e between 0.17 and $0.25 \text{ cm}^2/\text{s}$. The smallest relative width distributions occurred in two females of small stature. The diffusion maps of some healthy volunteers reveal that D_e is a slowly varying function of location within the lung. As the present technique determines D_e from a ratio of images, this spatial variation cannot be an artifact from inhomogeneous RF field, but must be physiological in origin. Upon partial exhalation, \overline{D}_e decreases slightly and the fractional width of the D_e distribution increases.

Five patients with severe emphysema were studied. The mean diffusivity \overline{D}_e in the patients is approximately 2.5 times that of the healthy volunteers. This is the most important result, confirming our hypothesis. Most of the patients display diffusivity histograms which are substantially broader than those of the healthy volunteers. However, the relative widths, $\Delta D_e/\overline{D}_e$, are similar in the two groups. The histograms do not, however, include regions of the lung which are the most poorly ventilated (such as the apices), so the histograms do not represent all lung volume elements. For the patients, some regions of high D_e

do not appear different in the spin density images from nearby regions of lower D_e . On the other hand, many patients show a correlated trend toward higher D_e and lower spin density as one ascends towards the apices.

Thus, imaging of ^3He effective diffusivity has the potential to identify regions of emphysematous tissue. In particular, one can characterize the status of lung regions before the disease has so advanced that these regions are not ventilated.

ACKNOWLEDGMENTS

The research was supported in part by a grant from the Whitaker Foundation to B.T.S. We acknowledge the assistance of Glenn Foster, and helpful discussions and preliminary experiments with J.J.H. Ackerman and Victor Song. A gift of free imaging hours from the Department of Radiology is appreciated.

REFERENCES

- Chen XJ, Chawla MS, Hedlund LW, Möller HE, MacFall JR, Johnson GA. MR microscopy of lung airways with hyperpolarized ^3He . *Magn Reson Med* 1998;39:79–84.
- de Lange EE, Mugler JP III, Brookeman JR, Knight-Scott J, Truwitt JD, Teates CD, Daniel TM, Bogorad PL, Cates GD. Lung air spaces: MR imaging evaluation with hyperpolarized ^3He gas. *Radiology* 1999;210:851–857.
- Kauczor H-U, Ebert M, Kreitner K-F, Nilgens H, Surkau R, Heil W, Hofmann D, Otten EW, Thelen M. Imaging of the lungs using ^3He MRI: preliminary clinical experience in 18 patients with and without lung disease. *J Magn Reson Imaging* 1997;7:538–543.
- Saam B, Yablonskiy DA, Gierada DS, Conradi MS. Rapid imaging of hyperpolarized gas using EPI. *Magn Reson Med* 1999;42:507–514.
- Chen XJ, Möller HE, Chawla MS, Cofer GP, Driehuys B, Hedlund LW, Johnson GA. Spatially resolved measurements of hyperpolarized gas properties in the lung in vivo. I. Diffusion coefficient. *Magn Reson Med* 1999;42:721–728.
- Chen XJ, Möller HE, Chawla MS, Cofer GP, Driehuys B, Hedlund LW, MacFall JR, Johnson GA. Spatially resolved measurements of hyperpolarized gas properties in the lung in vivo. II. T_2^* . *Magn Reson Med* 1999;42:729–737.
- Mugler JP III, Brookeman JR, Knight-Scott J, Maier T, de Lange EE, Bogorad PL. Regional measurement of the ^3He diffusion coefficient in the human lung. In: *Proc ISMRM, 6th Annual Meeting, Sydney, 1998*. p 1906.
- Braker W, Mossman AL. *Matheson gas data book*, 6th ed. Lyndhurst, NJ: Matheson. 1980.
- Barbé R, Leduc M, Laloë F. Résonance magnétique en champ de radiofréquence inhomogène 2^e partie: Vérifications expérimentales; mesure du coefficient de self-diffusion de ^3He . *J Physique* 1974;35:935–951.
- Liner JC, Weissman S. Determination of the temperature dependence of gaseous diffusion coefficients using gas chromatographic apparatus. *J Chem Phys* 1972;56:2288–2290.
- Yabsley MA, Dunlop PJ. A study of the two-bulb method for measuring diffusion coefficients of binary gas mixtures. *Physica* 1976;85A:160–174.
- Bear J. *Dynamics of fluids in porous media*. New York: American Elsevier; 1972. p 109–113.
- Sen PN, Schwartz LM, Mitra PP, Halperin BI. Surface relaxation and the long-time diffusion coefficient in porous media: periodic geometries. *Phys Rev* 1994;B49:215–225.
- Mair R, Wong G, Hoffmann D, Patz S, Hürlimann M, Schwartz L, Walsworth R. Time-dependent noble gas diffusion NMR in porous media and implications for lung study. In: *Proc ISMRM, 7th Annual Meeting, Philadelphia, 1999*. p 1799.
- Walker TG, Happer W. Spin-exchange optical pumping of noble-gas nuclei. *Rev Mod Phys* 1997;69:629–642.
- Karlicek RF Jr, Lowe JJ. A modified pulsed gradient technique for measuring diffusion in the presence of large background gradients. *J Magn Reson* 1980;37:75–91.
- West JB. *Pulmonary pathophysiology*, 4th ed. Baltimore: Williams and Wilkins; 1992. p 59.
- Slone RM, Gierada DS. Radiology of pulmonary emphysema and lung volume reduction surgery. *Semin Thorac Cardiovas Surg* 1996;8:61–82.
- Chen XJ, Hedlund LW, Chawla MS, Möller HE, Johnson GA. Detection of elastase-induced emphysema in rat lungs by measuring diffusion of hyperpolarized ^3He . In: *Proc ISMRM, 7th Annual Meeting, Philadelphia, 1999*. p 130.
- Schreiber WG, Markstaller K, Kauczor H-U, Surkau R, Eberle B, Großmann T, Weiler N, Otten E, Thelen M. Ultrafast imaging of lung ventilation using hyperpolarized Helium-3. In: *Proc ISMRM, 7th Annual Meeting, Philadelphia, 1999*. p 129.